Composite Nano-Antenna Integrated With Quantum Cascade Laser

Dibyendu Dey, *Student Member, IEEE*, John Kohoutek, *Student Member, IEEE*, Ryan M. Gelfand, *Student Member, IEEE*, Alireza Bonakdar, *Student Member, IEEE*, and Hooman Mohseni, *Senior Member, IEEE*

***Abstract*—Exploiting optical nano-antennas to boost the near-field confinement within a small volume can increase the limit of molecular detection by an order of magnitude. We present a novel antenna design based on Au–SiO_2–Au single nanorod integrated on the facet of a quantum cascade laser operating in the midinfrared region of the optical spectrum. Finite-difference time-domain simulations showed that for sandwiched dielectric thicknesses within the range of 20–30 nm, peak optical intensity at the top of the antenna ends is 500 times greater than the incident field intensity. The device was fabricated using focused ion beam milling. Apertureless midinfrared near-field scanning optical microscopy showed that the device can generate a spatially confined spot within a nanometric size about 12 times smaller than the operating wavelength. Such high intensity, hot spot locations can be used in increasing photon interaction with bio-molecules for sensing applications.**

***Index Terms*—Bio-sensing, field enhancement, near-field scanning microscopy, plasmonic antenna, quantum cascade laser (QCL).**

I. Introduction

SINCE its first demonstration [1] in 1994, the quantum cascade laser (QCL) has shown path breaking performance in terms of wall-plug efficiency [2], [3] and is currently considered one of the most efficient sources in the midinfrared (MWIR) region of optical spectrum. In its region of operation, several bio and chemical molecules have significant absorption, and thus building bio sensors based on QCL is highly desired. But unfortunately, due to several orders of magnitude dimensional difference between the lasing wavelength and the size of probed molecules, the light-particle interaction comes out to be very weak and it has remained the primary challenge in building sensitive midIR bio-sensors. The problem can be overcome by using optical nano antennas [4], [5], which are capable of focusing radiant infrared light down to nanometer lengths scale. Previously demonstrated nano antennas integrated with QCL have shown strong near-field enhancement but they were based on metal design [6], [7]. Composite noble-metal dielectric-based antenna introduces the novelty of having an increased number of regions with local "hot spots" due to a higher number of geometrical singularities. It also opens up the possibility to functionalize the multilayer—a feature extremely useful in bio-sensing applications [8]. Here we demonstrate a composite material-based optical antenna integrated with QCL that has a considerably higher peak intensity enhancement compared to metal design.

Manuscript received June 28, 2010; revised August 10, 2010; accepted August 27, 2010. Date of publication September 07, 2010; date of current version October 08, 2010. This work was supported in part by the National Science Foundation (NSF) under Grant CBET-0932611.

The authors are with the Department of Electrical Engineering and Computer Science, Northwestern University, Evanston, IL 60208 USA (e-mail: dey@u.northwestern.edu; johnkohoutek2008@u.northwestern.edu; ryangelfand2008@u.northwestern.edu; AlirezaBonakdar2015@u.northwestern.edu; hmohseni@ece.northwestern.edu).

Color versions of one or more of the figures in this letter are available online at http://ieeexplore.ieee.org.

Digital Object Identifier 10.1109/LPT.2010.2073459

II. Design

In order to accomplish the effective device design, we simulated the effect of each component of the integrated antenna using commercially available 3-D finite-difference time-domain (FDTD) software, Lumerical. All material data used in the simulation, other than the laser region, is from [9]. The refractive index of the laser material is chosen to be 3.2, which is the weighted average of the refractive index of the active region, $In_{0.44}Al_{0.56}As$–$In_{0.6}Ga_{0.4}As$.

To suppress unphysical reflections, the perfectly matched layers (PMLs) are used at the boundaries of the calculation region. The metal–dielectric–metal (MDM) nanorod design is illuminated using a transverse-magnetic (TM) polarized plane wave with a wavelength of 5.98 μm (operating wavelength of the device).

The incident electric field interacts with the free electrons of the metal and generates a polarization field. It leads to accumulation of opposite charges at the two ends of the nanorod. The built-up of charges generates strong near-field enhancement at the vicinity of the antenna ends. Due to the presence of sandwiched dielectric, the two vertically coupled Au-antennas interact with each other and it results in splitting the resonance into symmetric and antisymmetric modes [10].

To analyze the effect of sandwiched dielectric thickness, we calculated the peak intensity enhancement at the same level as the top metal surface near the edge of the antenna with varying dielectric thickness of 0, 5, 10, 20, 30, to 50 nm, while keeping the total thickness of the composite MDM layer constant at 170 nm. Fig. 1(a) shows that plot between peak intensity enhancement with varying antenna length and it shows that by increasing the SiO_2 thickness from 0 to 5 nm, the peak intensity is enhanced. It becomes 500 times the incident field intensity when the thickness of dielectric is in the range between 20 to 30 nm. This is a two-fold increase compared to metal antenna at its resonant length. Away from this optimum range, the peak intensity again starts to decrease. We believe transverse coupling of surface plasmon waves at the interface between a metal and

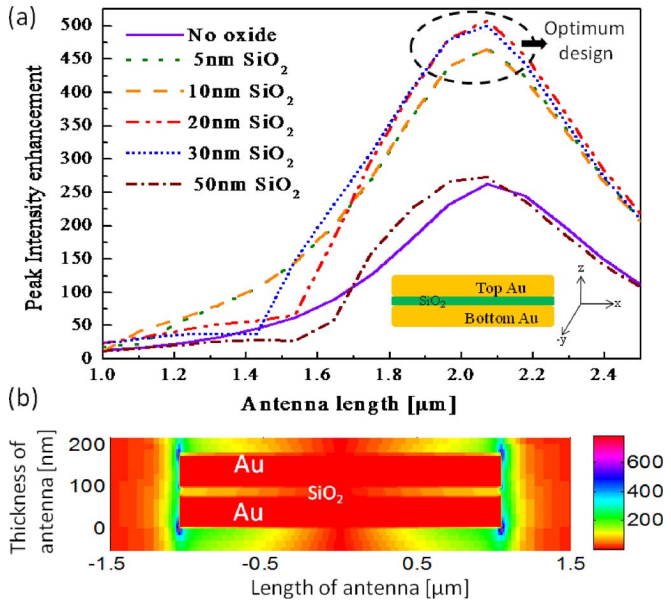

Fig. 1. (a) FDTD simulation shows the peak intensity enhancement versus antenna length at $\lambda = 5.98\ \mu$m. The silicon dioxide thickness for MDM structure has been varied from 0, 5, 10, 20, 30, to 50 nm, while keeping the total thickness of the structure to be constant at 170 nm. Inset: schematic diagram of the MDM single nanorod. (b) Simulated E-field intensity distribution of the $y = 0$ plane for MDM nanorod (Au–SiO_2–Au) at a resonant length of 2.0 μm. It also shows the location of multiple hot spots with high peak intensity ~ 500 times the incident field intensity.

a dielectric may be the possible reason for this increase in peak optical intensity as compared to a single metal design [11].

III. Fabrication and Measurement

We fabricated an optical antenna on an edge-emitting QCL operating at room temperature. The core design of the laser is based on $In_{0.44}Al_{0.56}As$–$In_{0.6}Ga_{0.4}As$ with a core design as outlined in a previous letter [12]. To prevent electrical shorting with the MDM antenna, an insulating buffer layer of 100 nm SiO_2 was first deposited on the facet of QCL using ebeam evaporation. Next, the Au–SiO_2–Au (75 nm/20 nm/75 nm) was deposited on the buffer silicon dioxide film. The rate of deposition was kept very low (0.1 nm/s), to decrease nonuniformity in layer thicknesses. Still, there was a fluctuation up to ± 4 nm. However, such nonuniformity can only cause some damping loss without affecting the near-field behavior of the antenna.

After that, the optimized antenna structure was defined on the multilayer film using a focused ion beam (Hellios FEI). The nanorod length was kept to be $\sim 2\ \mu$m and the width ~ 100 nm. A gallium ion beam at high voltage (30 keV) and low current (48 pA) was used to achieve a high precision of milling. Fig. 2 shows the scanning electron micrograph image of the fabricated nanorod. The device was electrically tested in pulsed mode with 1% duty cycle (100 ns, 100 KHz) and the threshold current was found to be 2.28 A (without antenna) and 1.65 A (with antenna). Other than reduction in threshold current (due to enhanced reflectivity from the coated facet), the fabricated antenna did not have a serious effect on the operation of the laser.

After fabricating the device, we experimentally measured the electric field enhancement using a near-field scanning optical microscope (NSOM) [13]. In this technique, the near-field

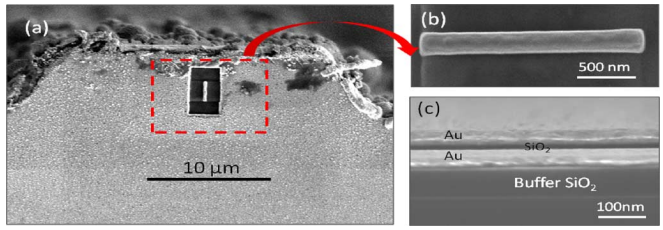

Fig. 2. (a) SEM image of the Au–SiO_2–Au (75/20/75 nm) single nanorod antenna integrated on the facet of QCL. (b) Top view of Au–SiO_2–Au (75/20/75 nm) single nanorod antenna. (c) Cross-sectional view of Au–SiO_2–Au (75/20/75 nm) layers of the antenna.

images and topography of the patterned QCL were simultaneously measured. Commercially available NSOMs generally use a spatially confined optical spot at the end of a hollow metallic scanning tip to selectively illuminate the probed surface to produce an image beyond the diffraction limit. However, this setup involves complicated intermediate optics and an external light source. In contrast, we set up a midinfrared NSOM (Fig. 3) based on a commercially available atomic force microscope (AFM) (Agilent 5400). The apex of the sharp platinum coated AFM tip scans the surface of the sample and scatters the local electromagnetic field coming from the antenna structure. The AFM cantilever was driven at its resonance oscillation frequency of 70 KHz. The scattered signal travels back through the laser cavity. After collimation through an objective lens, it gets collected by a mercury–cadmium telluride (MCT) detector. This scattered signal possesses local field information. However, there is also scattering from the cantilever, which produces a huge background noise. As the signal has a definite frequency band defined by the tapping mode frequency of the AFM, noise and signal can be separated using lock-in technique with a matching reference frequency. The resulting signal gives an image of the near-field intensity pattern of the fabricated antenna.

IV. Results

The near field of the antenna excites surface plasmons [14] to the AFM tip, which in turn radiates a signal detected by an infrared detector to generate NSOM image. In Fig. 4(b) and (c), the topography and near-field image of Au–SiO_2–Au (75/20/75 nm) nanorod antenna are shown. The NSOM image matches closely with the simulated E_z component of the electric field distribution shown in Fig. 4(a). In [15], a quasi-electrostatic theory has been used to calculate the radiated dipole field by the AFM tip and is found to be stronger for electric field perpendicular to the sample surface (E_z). This makes the direct comparison of near-field behavior between the recorded NSOM image and simulated E_z meaningful. However, a numerical matching between simulated and NSOM data might not be possible as the scattered light passes through the laser cavity and experiences nonlinear gain as well as the arbitrary gain involved during the lock-in technique.

The near-field images of the antenna were recorded with high pixel resolution and with a reduced scan speed of 0.1 lines/s. The image distortions, as seen in Fig. 4(b), are due to small drifts in sample position occurring over the long acquisition time for

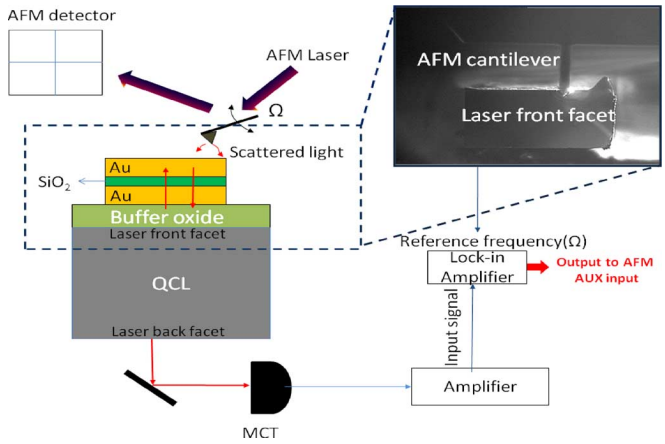

Fig. 3. (a) NSOM to simultaneously measure the topography and near-field intensity of the optical antenna. Inset: Optical microscope image of the laser facet along with the AFM tip in tapping mode.

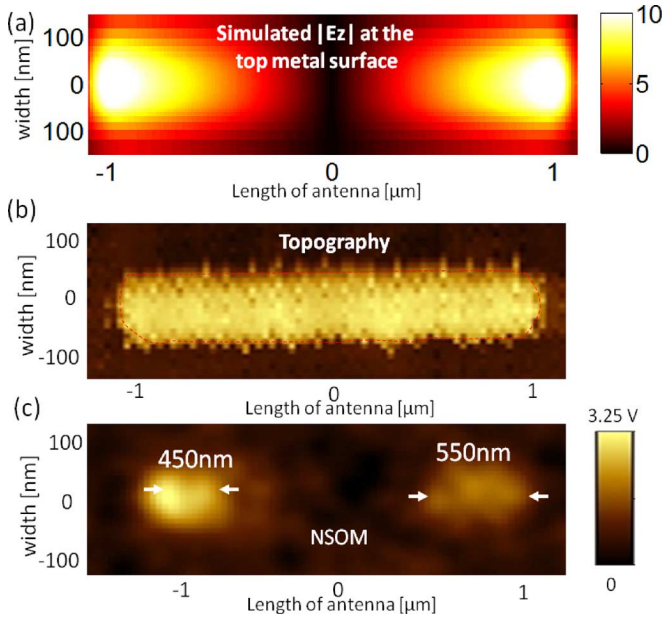

Fig. 4. (a) Simulated $|E_z|$ for the MDM nanorod antenna. (b), (c) Topography and NSOM image of the Au–SiO_2–Au single nanorod antenna integrated on the facet of a room-temperature working QCL.

NSOM measurement. When compared to the simulated results, the intensities at the two ends of the nanorod have been found to be nonidentical and it can be due to possible fabrication nonuniformity on the surface of the antenna caused by FIB.

During the NSOM measurement, the laser was operated at 1% duty cycle near the threshold voltage with an average power output of 100 μW. The full-widths at half-maximum of the two peak intensities at the edge of the antenna were found to be 450 and 550 nm, respectively [Fig. 4(c)]. This intense optical spot is localized within an area that is $\sim$ 12 times smaller than the operating wavelength. Based on our simulation, the peak intensity enhancement can be up to a factor of 500 and thus neglecting any incurred optical losses, there can be high power density inside the "hot spot" region.

V. Conclusion

We have demonstrated NSOM of an MDM nanorod antenna integrated on to the facet of a QCL. FDTD simulation results were used to optimize the dielectric thickness in the range of 20–30 nm. These simulations also indicate that at resonance, the peak intensity from the antenna can be up to 500 times the incident field intensity. Experiments have shown that the optical mode can be squeezed within a nanometric spot size $\sim$500 nm on the top of the antenna ends. The NSOM images have good agreement with the simulated z-component of the near-field distribution. Such an integrated plasmonic laser antenna can be useful in making sensitive bio-sensors [16]–[18].

References

[1] J. Faist, F. Capasso, D. L. Sivco, C. Sirtori, A. L. Hutchinson, and A. Y. Cho, "Quantum cascade laser," *Science*, vol. 264, pp. 553–556, Apr. 1994.

[2] Y. Bai, S. Slivken, S. Kuboya, S. R. Darvish, and M. Razeghi, "Quantum cascade laser that emits more light than heat," *Nat. Photonics*, vol. 4, pp. 99–102, Jan. 2010.

[3] P. Q. Liu, A. J. Hoffman, M. D. Escarra, K. J. Franz, J. B. Khurgin, Y. Dikmelik, X. Wang, J.-Y. Fan, and C. F. Gmachl, "High power efficient quantum cascade," *Nat. Photonics*, vol. 4, no. 98, Jan. 2010.

[4] J. Alda, J. M. Rico-Garcia, J. M. Lopez, and G. Boreman, "Optical antennas for nano-photonic applications," *Nanotechnology*, vol. 16, pp. S230–S234, Mar. 2005.

[5] X. Xu, E. X. Jin, L. Wang, and S. Uppuluri, "Design, fabrication and characterization of nanometer-scale ridged aperture optical antenna," *Proc. SPIE*, vol. 6106, p. 61061J, Mar. 2006.

[6] N. Yu, E. Cubukcu, L. Diehl, M. A. belkin, K. B. Crozier, and F. Capasso, "Plasmonic quantum cascade laser antenna," *Appl. Phys. Lett.*, vol. 91, pp. 173113–173116, Oct. 2007.

[7] E. Cubukcu, N. Yu, E. J. Smythe, L. Diehl, K. B. Crozier, and F. Capasso, "Plasmonic laser antenna and related device,s," *IEEE J. Sel. Quantum Electron.*, vol. 14, no. 6, pp. 1448–1461, Dec. 2008.

[8] E. katz and I. Willner, "Integrated nanoparticle-biomolecule hybrid system : Synthesis, properties and applications," *Angewandte*, vol. 43, pp. 6042–6108, Nov. 2004.

[9] D. Palik, *Handbook of Optical Constants of Solids*. New York: Academic, 1985.

[10] L. Wang, J. Zhang, X. Wu, J. Yang, and Q. Gong, "Resonances of sandwiched optical antenna," *Opt. Commun.*, vol. 21, pp. 5444–5447, Nov. 2008.

[11] D. Dey, J. Kohoutek, R. M. Gelfand, A. Bonakdar, and H. Mohseni, "Quantum cascade laser integrated with metal-dielectric-metal based plasmonic antenna," *Opt. Lett.*, vol. 35, pp. 2783–2785, Aug. 2010.

[12] L. Diehl, D. Bour, S. Corzine, J. Zhu, G. Hofler, M. Loncar, M. Troccoli, and F. Capasso, "High-temperature continous wave operation of strain-balanced quantum cascade lasers grown by metal organic vapor-phase epitaxy," *Appl. Phys. Lett.*, vol. 83, pp. 3245–3248, Aug. 2003.

[13] J. Kim and K.-B. Song, "Recent progress of nano-technology with NSOM," *Micron*, vol. 38, pp. 409–426, Jul. 2006.

[14] H. Raether, *Surface Plasmons on Smooth and Rough Surfaces and on Gratings*. Berlin, Germany: Springer-Verlag, 1998, ch. 2.

[15] M. Knoll and F. Keilmann, "Enhanced dielectric contrast in scattering-type scanning near-field optical microscopy," *Opt. Commun.*, vol. 182, pp. 321–328, Aug. 2000.

[16] M. F. Garcia-Parajo, "Optical antenna focusing in on biology," *Nat. Photonics*, vol. 2, pp. 201–203, Apr. 2008.

[17] J. Alda, J. M. Rico-García, J. M. López-Alonso, and G. Boreman, "Optical antennas for nano-photonic applications," *Nanotechnology*, vol. 16, pp. S230–S234, Mar. 2005.

[18] S. S. Aimovi, M. P. Kreuzer, M. U. González, and R. Quidant, "Plasmonic near field coupling in metal dimmers as a step towards single molecule sensing," *ACS Nano*, vol. 3, pp. 1231–1237, Apr. 2009.